Acta Biomaterialia 140 (2022) 389–397

Contents lists available at ScienceDirect

Acta Biomaterialia

journal homepage: www.elsevier.com/locate/actbio

Full length article

Microscopic multifrequency magnetic resonance elastography of *ex vivo* abdominal aortic aneurysms for extracellular matrix imaging in a mouse model

Dilyana B. Mangarova[a,b,*], Gergely Bertalan[a], Jakob Jordan[a], Julia Brangsch[a], Avan Kader[a,c], Jana Möckel[a], Lisa C. Adams[a], Ingolf Sack[a], Matthias Taupitz[a], Bernd Hamm[a], Marcus R. Makowski[a,e,1], Jürgen Braun[a,d,1]

[a] *Department of Radiology, Charité – Universitätsmedizin Berlin, corporate member of Freie Universität Berlin, Humboldt-Universität zu Berlin, and Berlin Institute of Health, Charitéplatz 1, Berlin 10117, Germany*
[b] *Department of Veterinary Medicine, Institute of Veterinary Pathology, Freie Universität Berlin, Robert-von-Ostertag-Str. 15, Building 12, Berlin 4163, Germany*
[c] *Department of Biology, Chemistry and Pharmacy, Institute of Biology, Freie Universität Berlin, Königin-Luise-Str. 1-3, Berlin 14195, Germany*
[d] *Institute for Medical Informatics, Charité - Universitätsmedizin Berlin, Berlin, Germany, corporate member of Freie Universität Berlin, Humboldt-Universität zu Berlin, and Berlin Institute of Health, Hindenburgdamm 30, Berlin 12200, Germany*
[e] *Department of Diagnostic and Interventional Radiology, Technical University of Munich, Ismaninger Str. 22, Munich 81675, Germany*

ARTICLE INFO

Article history:
Received 6 August 2021
Revised 16 November 2021
Accepted 17 November 2021
Available online 21 November 2021

Keywords:
Magnetic resonance elastography
Proof-of-concept
AAA
Stiffness

ABSTRACT

An abdominal aortic aneurysm (AAA) is a permanent dilatation of the abdominal aorta, usually accompanied by thrombus formation. The current clinical imaging modalities cannot reliably visualize the thrombus composition. Remodeling of the extracellular matrix (ECM) during AAA development leads to stiffness changes, providing a potential imaging marker. 14 apolipoprotein E-deficient mice underwent surgery for angiotensin II-loaded osmotic minipump implantation. 4 weeks post-op, 5 animals developed an AAA. The aneurysm was imaged *ex vivo* by microscopic multifrequency magnetic resonance elastography (μMMRE) with an in-plane resolution of 40 microns. Experiments were performed on a 7-Tesla preclinical magnetic resonance imaging scanner with drive frequencies between 1000 Hz and 1400 Hz. Shear wave speed (SWS) maps indicating stiffness were computed based on tomoelastography multifrequency inversion. As control, the aortas of 5 C57BL/6J mice were examined with the same imaging protocol. The regional variation of SWS in the thrombus ranging from 0.44 ± 0.07 to 1.20 ± 0.31 m/s was correlated fairly strong with regional histology-quantified ECM accumulation (R^2 = 0.79). Our results suggest that stiffness changes in aneurysmal thrombus reflect ECM remodeling, which is critical for AAA risk assessment. In the future, μMMRE could be used for a mechanics-based clinical characterization of AAAs in patients.

Statement of significance

To our knowledge, this is the first study mapping the stiffness of abdominal aortic aneurysms with microscopic resolution of 40 μm. Our work revealed that stiffness critically changes due to extracellular matrix (ECM) remodeling in the aneurysmal thrombus. We were able to image various levels of ECM remodeling in the aneurysm reflected in distinct shear wave speed patterns with a strong correlation to regional histology-quantified ECM accumulation. The generated results are significant for the appli-

* Corresponding author at: Department of Radiology, Charité – Universitätsmedizin Berlin, corporate member of Freie Universität Berlin, Humboldt-Universität zu Berlin, and Berlin Institute of Health, Charitéplatz 1, Berlin 10117, Germany.
E-mail addresses: dilyana.mangarova@charite.de (D.B. Mangarova), gergely.bertalan@charite.de (G. Bertalan), jakob.jordan@charite.de (J. Jordan), julia.brangsch@charite.de (J. Brangsch), avan.kader@charite.de (A. Kader), jana.moeckel@charite.de (J. Möckel), lisa.adams@charite.de (L.C. Adams), ingolf.sack@charite.de (I. Sack), matthias.taupitz@charite.de (M. Taupitz), bernd.hamm@charite.de (B. Hamm), marcus.makowski@charite.de (M.R. Makowski), juergen.braun@charite.de (J. Braun).
[1] These authors contributed equally to this work.

https://doi.org/10.1016/j.actbio.2021.11.026

cation of microscopic multifrequency magnetic resonance elastography for quantification of pathological remodeling of the ECM and may be of great interest for detailed characterization of AAAs in patients.

1. Introduction

An abdominal aortic aneurysm (AAA) is a degenerative vascular disease of the aorta with mortality rates of up to 90% in case of rupture [1]. Factors that lead to AAA rupture are not yet fully understood, and diagnostic medical imaging is mainly based on the anatomical representation of AAAs. In clinical practice, the aneurysmal thrombi in human patients are diagnosed by ultrasound [2], computed tomography [3], or magnetic resonance imaging (MRI) [4]. Based on the long-standing assumption that AAAs rupture risk is positively correlated to size [5–7], the size criterion still serves as the basis for deciding on surgical intervention [8].

There is growing evidence that rupture risk involves various factors related to the biomechanical properties of AAAs and that stiffness plays a central role in AAA expansion and rupture potential [9]. It is well-known that in healthy aortas, proper connective protein density and intact extracellular matrix (ECM) network are the basis for reversible extensibility during the cardiac cycle and wall stability under high stress [10,11]. AAAs are formed under progressive extracellular matrix (ECM) remodeling, mainly characterized by elastin degradation and distortion [12,13]. Consistently, ruptured AAAs show an even more progressed decrease in elastin than unruptured AAAs [13].

An essential aspect of the aforementioned alterations in the ECM content is the aneurysmal thrombus. Intraluminal thrombi (ILTs) are present in the majority of larger human AAAs [14]. Stiffer, well-organized thrombi lead to reduced wall stress in comparison to pliant, less-organized thrombi [15,16]. On the other hand, ILTs can indirectly weaken the arterial wall by causing hypoxia and promoting neovascularization, infiltration with inflammatory cells and enzymes [17,18]. Moreover, fissures in the ILT, especially those that connect the lumen with the aortic wall and/or comprise a substantial volume of the thrombus mass, increase arterial wall stress [19] and may thus facilitate AAAs rupture.

To study the underlying mechanisms and altered mechanical tissue parameters for improved diagnosis and prediction of AAA rupture risk, a direct, imaging-based measurement of the stiffness of the AAA would be beneficial. Elastography comprises medical imaging techniques such as MRI and ultrasound extended by mechanical vibrations in the audible range to induce shear waves and inversion algorithms to recover stiffness maps from shear wave patterns [20]. Unlike light-based techniques such as microscopy, the resolution of elastography techniques depends on the accuracy of the measurement of wave gradients, which does not necessarily increase with excitation frequency, but with the signal-to-noise ratio (SNR) of the imaging technique [21]. Recent studies have shown the feasibility and potential of magnetic resonance elastography (MRE) [22–31] and ultrasound elastography (USE) [32–40] for quantifying aortic and AAA stiffness. However, these studies were mainly limited in spatial resolution and focused on humans [22,25–28,30–32,34,35,37,39] or large animal models [23,24,29,33,36,38,40].

So far, preclinical MRE can provide maps of viscoelastic parameters with a spatial resolution on the order of 150 µm [41,42]. With microscopic magnetic resonance elastography (µMRE) 34 µm pixel size was reported without mapping the heterogeneity of viscoelastic parameters [43]. We hypothesize that the highly heterogeneous structure of AAA requires high resolutions MRE which can be achieved with multifrequency inversion methods which have been proven robust for mapping stiffness details in soft tissues *in vivo* and *ex vivo* [44,45]. Therefore, we here combine µMRE with multifrequency wave acquisition and reconstruction (µMMRE) to arrive, for the first time, at stiffness maps with in-plane pixel sizes of 40×40 µm^2.

This study is pursuing two objectives: First, to demonstrate the feasibility of µMMRE to generate high-spatial resolution stiffness maps in *ex vivo* samples of an AAA mouse model. Second, to compare µMMRE stiffness maps with histological stainings of ECM proteins to evaluate the potential use of AAA stiffness as a quantitative biomarker of rupture risk.

2. Methods

2.1. Animal model

The animal experiments were approved and performed according to the animal protection committee of the LaGeSo, Berlin, Germany, the local Guidelines and Provisions for Implementation of the Animal Welfare Act by Charité - Universitätsmedizin Berlin and the regulations of the Federation of Laboratory Animal Science Associations (FELASA).

The surgery protocol in this study is as described in previous publications from our group [46,47]. In short, 8-weeks old B6.129P2-*Apoetm1Unc/J* (ApoE-/-) male mice underwent surgical implantation of osmotic minipumps ($N = 14$). The animals were anesthetized by intraperitoneal (i.p.) application of 500 µg/kg medetomidine, 50 µg/kg fentanyl, and 5 mg/kg midazolam. The anesthesia was reverted post-operative by i.p. combination of atipamezole (2.5 mg/kg), naloxone (1.2 µg/kg) and flumazenil (500 µg/kg). Angiotensin II-filled osmotic minipumps (Alzet model 2004, Durect Corp, Cupertino, CA, USA) with an infusion rate of 1000 ng/kg/min were implanted subcutaneously in the dorsal neck area [48]. Four weeks later, the animals were euthanized by cervical dislocation, underwent cardiac perfusion with saline, the abdominal portion of the aorta was dissected [49] and µMMRE was performed directly afterwards. Additionally, 5 C57BL/6J healthy male mice were euthanized at 12 weeks of age and followed the same imaging protocol. Our control group consists of C57BL/6J mice and not ApoE-/- mice, because the ApoE-/- strain could potentially develop cardiovascular pathologies even under normal housing and dietary conditions [50].

2.2. Sample preparation

The abdominal portion of the aorta was separated from the surrounding tissue. In order to prevent the lumen from collapsing, ligatures tying off both ends of the isolated artery were completed after perfusion, one in the renal region and one approximately 1.0 cm further cranial. By using the free ends of the suture material, the samples were navigated into the 3.2 mm inner diameter glass tube (Wilmad Lab Glass, Buena, NJ, USA) parallel to the wall and consequently embedded in ultrasound gel with a SWS of 0.77 ± 0.09 m/s between 1000 and 1400 Hz [51] (Gello GmbH Geltechnik, Ahaus, Germany) using a 20G cannula (B Braun, Melsungen, Germany) (Fig. 1).

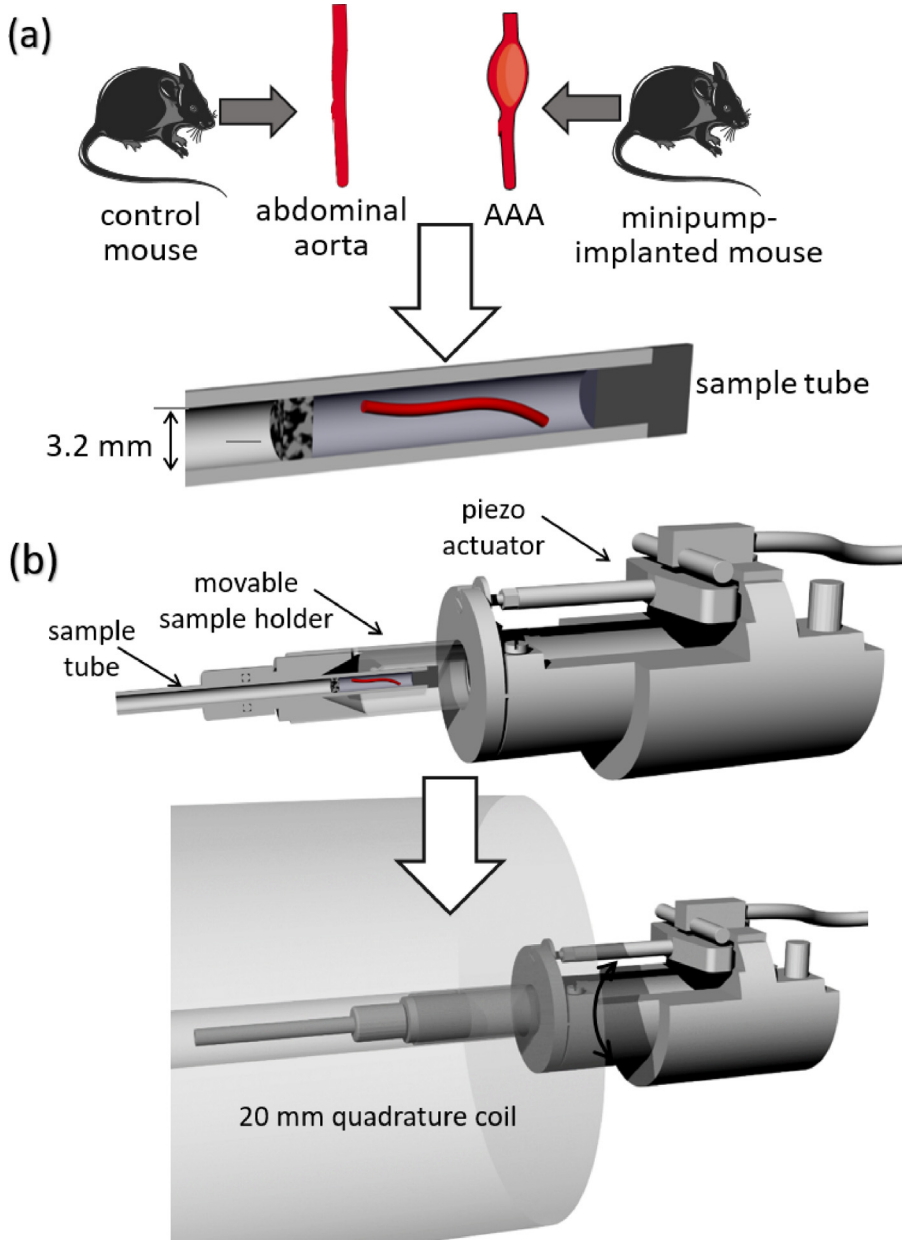

Fig. 1. Experimental setup. Apolipoprotein E-deficient mice underwent surgery for angiotensin II-filled osmotic minipump implantation ($N = 14$). **(a)** Four weeks later, five animals developed an abdominal aortic aneurysm ($n = 5$), the abdominal aorta was dissected and inserted into a 3.2 mm, ultrasound gel-filled glass sample tube. **(b)** µMMRE was conducted on a 7 T preclinical small animal MRI scanner using a 20 mm-diameter quadrature volume coil. For the control group, the aortas of C57BL/6J mice ($n = 5$) were dissected and underwent the same imaging protocol described above. *µMMRE* microscopic multifrequency magnetic resonance elastography, *MRI* magnetic resonance imaging.

2.3. Histology

Following *ex vivo* µMMRE, the aortic samples were embedded in optimal cutting temperature compound (Sakura Finetek, Torrance, CA, USA) at −25° in the same transverse orientation as for µMMRE imaging, frozen and cryosectioned at 14 µm thickness. The samples were than processed with Miller's Elastica van Gieson (EvG), Hematoxylin and Eosin (H&E) and Picrosirius red (PSR) histology stains. The resulting slices were scanned and photographed using a light microscope (Keyence BZ-X800, Keyence Ltd. HQ & Laboratories, Osaka, Japan). For collagen quantification by PSR, a polarizing filter (Daitron Co. Ltd, Tokyo, Japan) was inserted to the microscope to measure fiber birefringence. The morphometric analysis of the aortic region was performed using Keyence BZ-X800 Analyzer software (Keyence BZ-X800, Keyence Ltd. HQ & Laboratories, Osaka, Japan). To measure the ECM content in a single digitized image, the color profile of collagen and elastin as seen using PSR and EvG, respectively, was set as reference. All structures within this specific color profile were automatically recorded and divided by the overall tissue area of the aorta in order to acquire the collagen or elastin concentration. In addition, we set regions of interest in the thrombus representing ECM-rich and ECM-poor areas and measured the local collagen and elastin concentration. In order to detect local ECM variations, multiple transverse slides from each aorta were analyzed.

2.4. Microscopic multifrequency magnetic resonance elastography

µMMRE of tissue samples was conducted on a 7 T preclinical small animal MRI scanner (Bruker Biospec, Ettlingen, Germany;

Paravision 6.0.1) using a 20 mm-diameter ^{1}H-RF quadrature volume coil (RAPID Biomedical, Würzburg, Germany) at 23 ± 0.5 °C. Mechanical oscillations with 1000, 1100, 1200, 1300 and 1400 Hz frequencies were induced into the sample as shown in Fig. 1b by a custom-made driver setup [44]. Wave images were acquired in a transverse view using a multi-shot spin-echo MRE sequence equipped with sinusoidal motion encoding gradients (MEGs) in direction of the slice select axis of the scanner. The frequencies of the MEGs were identical to the vibration frequencies, respective MEG numbers and amplitudes (in mT/m) were: 11, 320mT/m | 1000 Hz, 11, 320 mT/m | 1100 Hz, 12, 320 mT/m | 1200 Hz, 13, aa | 1300 Hz, 14, 320 mT/m | 1400 Hz. Further acquisition parameters were: repetition time (TR): 2000 ms, echo time (TE): 31 ms, field of view (FoV): 4.0 × 4.0 mm^2, matrix size: 100 × 100, in-plane resolution 40 × 40 µm^2, and slice thickness: 0.7 mm. The total acquisition time for all 5 vibration frequencies, each of which sampled with 4 wave dynamics, was approximately 1 h per sample. Shear wave speed (SWS in m/s) maps as a marker of stiffness were calculated from the complex-valued wave images after phase unwrapping and temporal Fourier transformation of the four wave dynamics using multifrequency wave-number inversion (k-MDEV). In previous work, we have validated the inversion algorithm by a similar µMMRE technique used herein applied to homogeneous ultrasound gel [51]. The entire postprocessing pipeline is open-access under https://bioqic-apps.charite.de.

2.5. Statistical analysis

Values are specified as mean±SD. A Student's t-test (unpaired, 2-tailed) was applied. Following continuous variables were compared: size, SWS, amount of collagen, amount of elastin. For significance testing, a p-value < 0.05 was considered to indicate a statistically significant difference.

3. Results

3.1. AAA development and morphometry

In the experimental group, 5 out of the 14 animals that underwent surgery developed an AAA, the animals that did not develop an AAA ($n = 4$) or suffered a rupture ($n = 5$) were excluded from the study prior to data acquisition. 3 of the AAAs were accompanied by the formation of a large thrombus while 2 AAAs did not develop a pronounced thrombus. We observed no AAA development in the control group.

Cross sections of the abdominal aorta were examined after 4 weeks of Ang II-infusion by µMMRE and histology. We observed a significant dilatation ($p < 0.05$) with an average luminal aortic area of 0.52 mm^2 in the AAA group after 4 weeks of infusion in comparison to an area of 0.29 mm^2 in the control group (Fig. 2).

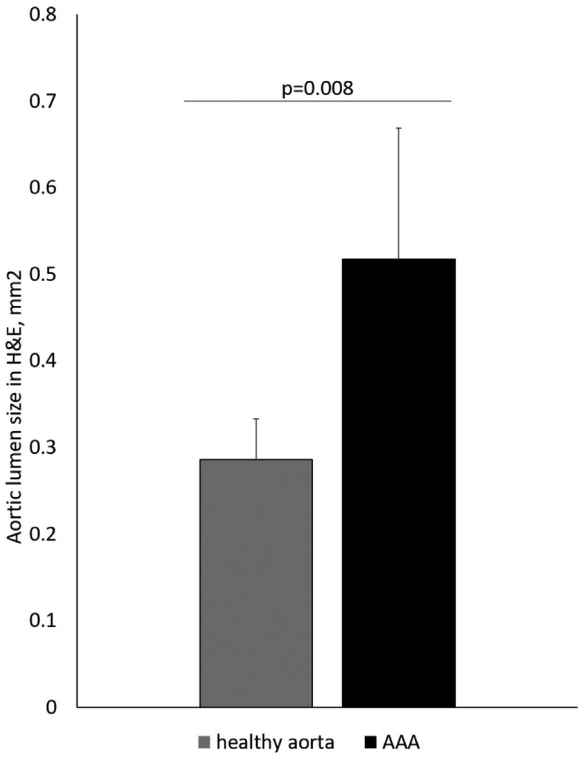

Fig. 2. AAA development. A pronounced dilatation of the aortic lumen was observed in histology between the control group and AAA group ($p = 0.008$). *AAA* abdominal aortic aneurysm, *H&E* hematoxylin-eosin stain.

3.2. Microscopic multifrequency magnetic resonance elastography

To evaluate the potential of µMMRE as a tool for AAA characterization, we performed *ex vivo* examinations of different regions of the thrombus. Fig. 3a shows representative wave images for a control aorta and for an AAA, both embedded in ultrasound gel for all recorded frequencies. MRE magnitude images and SWS maps with an in-plane resolution of 40 µm calculated by k-MDEV are shown for a control aorta and an AAA in Fig. 3b, respectively.

3.3. Correlation of stiffness with ECM protein content and distribution

Fig. 4 shows a comparison between μMMRE based spatially high resolved SWS maps (row 1) and histological stainings for AAAs with (columns b, c, d) and without (column e) a pronounced thrombus, as well as a healthy aorta (column a). For an overview of tissue structure, H&E staining was acquired (row 2). To investigate the spatial distribution and concentration of ECM proteins in AAA and healthy aortas, EvG (row 3) and PSR (row 4) stainings were performed to assess elastin and collagen content, respectively. Strong matrix remodeling is evident, with inhomogeneity of the thrombus that was characterized by distinct ECM-rich and ECM-poor regions (columns b, c, d). In addition, there was a strong spatial overlap between regional collagen and elastin content.

Based on the EvG and PSR stainings (row 3 and row 4, respectively, in Fig. 4), regional analysis of SWS for ECM-rich and ECM-poor regions of three thrombi revealed significant different mean stiffness ($p < 0.05$) based on mean SWS of 1.04 m/s (SD = 0.31) and 0.44 m/s (SD = 0.07) shown in Fig. 5a. When comparing ROIs demarcating ECM-rich and -poor areas of the thrombus in SWS maps and histology, SWS values correlated greatly with both elastin ($R^2 = 0.79$) and collagen ($R^2 = 0.79$) content separately and collectively ($R^2 = 0.80$) (Fig. 5c–e). Moreover, when comparing the SWS maps to H&E staining of the same transverse aortic regions, there was a fairly strong positive correlation in lumen diameter ($R^2 = 0.71$) (Fig. 5f) as well as total AAA size, including the area of the thrombus ($R^2 = 0.70$) (Fig. 5g).

4. Discussion

This is the first study to investigate the use of μMMRE for imaging AAAs in a small animal model. Under *ex vivo* conditions, maps of SWS as a surrogate marker for stiffness with a spatial resolution of 40 × 40 μm could be obtained. By comparison, the highest spatial resolution achieved so far was reported for USE with 60 × 250 μm in axial / lateral sound wave direction for *ex vivo* investigations on porcine aortas. The diameters of the lumen and the total AAA size based on H&E stainings and stiffness

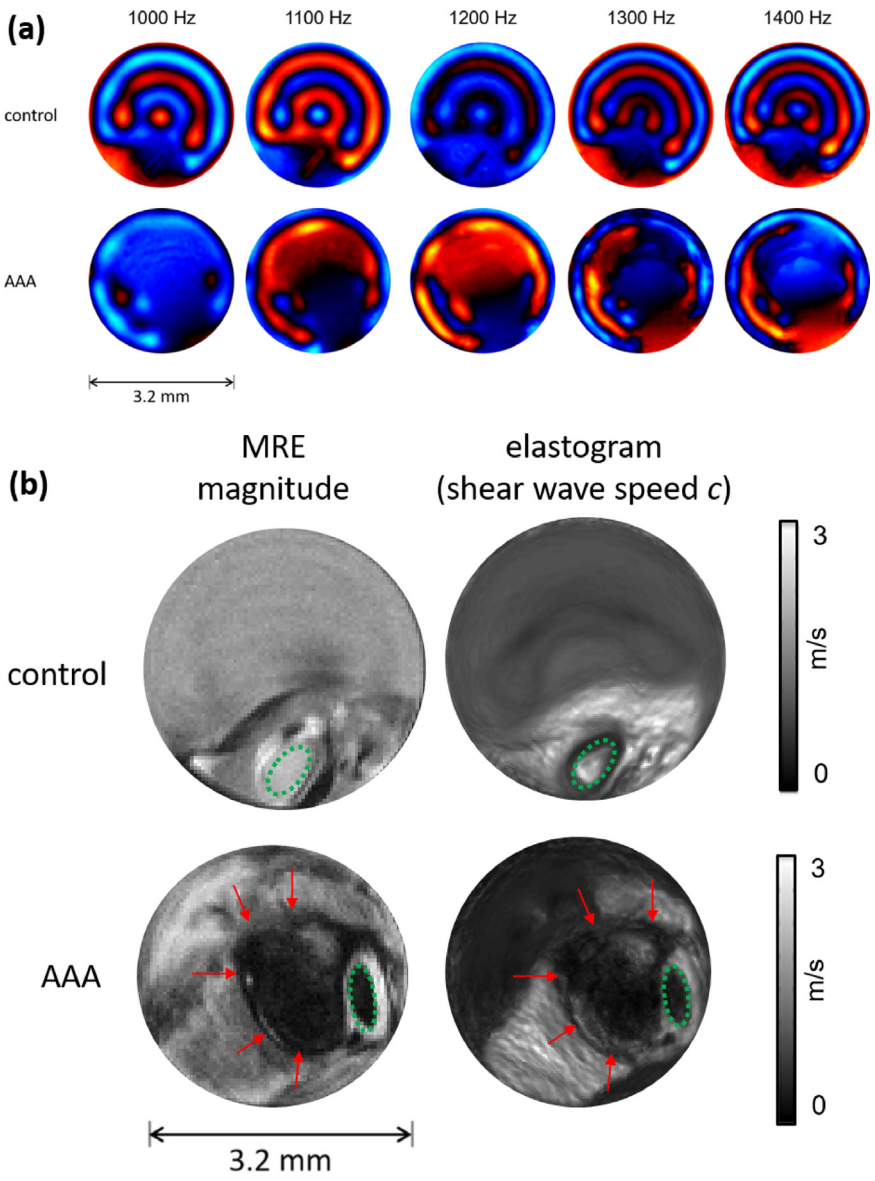

Fig. 3. *Ex vivo* microscopic multifrequency magnetic resonance elastography. **(a)** A custom-made driver setup was used to induce mechanical oscillations with 1000, 1100, 1200, 1300 and 1400 Hz frequencies into the specimen. **(b)** MRE magnitude and shear wave speed images of AAAs and healthy aortic vessels were acquired in a transversal view.

maps showed strong correlations ($R^2 = 0.71$, $R^2 = 0.70$) with a significant, almost doubled increase in lumen diameter from 0.29 to 0.52 mm^2 after 4 weeks of Ang II-infusion. This is in good agreement with published results on AAAs in the Ang II-infused mouse model [47]. While the absolute number of animals that developed an AAA in our study is smaller than normally described in the literature [48], it is important to note that 5 of the animals suffered a rupture during the first week after implantation, which is in line with the 10–30% mortality rate previously described [48]. Since 5 of the remaining 9 animals developed an AAA, our numbers are in line with the expected incidence of 50% or more [48].

The main focus of our current study was to provide local stiffness information of AAAs as a new biomarker for the estimation of rupture risk. The basis for this hypothesis is structural change of tissue in the formation of AAAs. While the pathogenesis of AAA development has not been fully elucidated, accompanying dysregulated tissue homeostasis is generally accepted [52]. In the arterial wall, elastolysis causes a shift of the mechanical load from elastic lamellae to collagen fibers that are 100 to 1000 times stiffer than elastin, leading to an increased risk for rupture [53]. The morphology and structure of the simultaneously forming thrombus has an additional influence on the occurrence of a rupture. In humans, thrombi can be highly heterogeneous. Individual areas may appear disorganized or show different consistency, thickness, stratification, microstructure and mechanical properties [14,54,55]. In this context, several types of blood-filled channels described as cavities, canaliculi, or fissures have been characterized [19,56,57]. In addition to these "holes," thrombus stability is reduced via inflammation-driven neovascularization [58]. Finally, concerning the rupture risk of arterial walls, there is a complex interplay between protective properties provided by a thick thrombus and likewise weakening by SMC apoptosis and ECM degradation [59,60].

These observations were confirmed by our histological analysis. Both total elastin and collagen quantity determined by Elastica-van-Gieson (EvG) and Picrosirius red (PSR) stainings, respectively, decreased significantly ($p < 0.05$) in AAAs compared to the control group. Thrombi were characterized by strong matrix remodeling

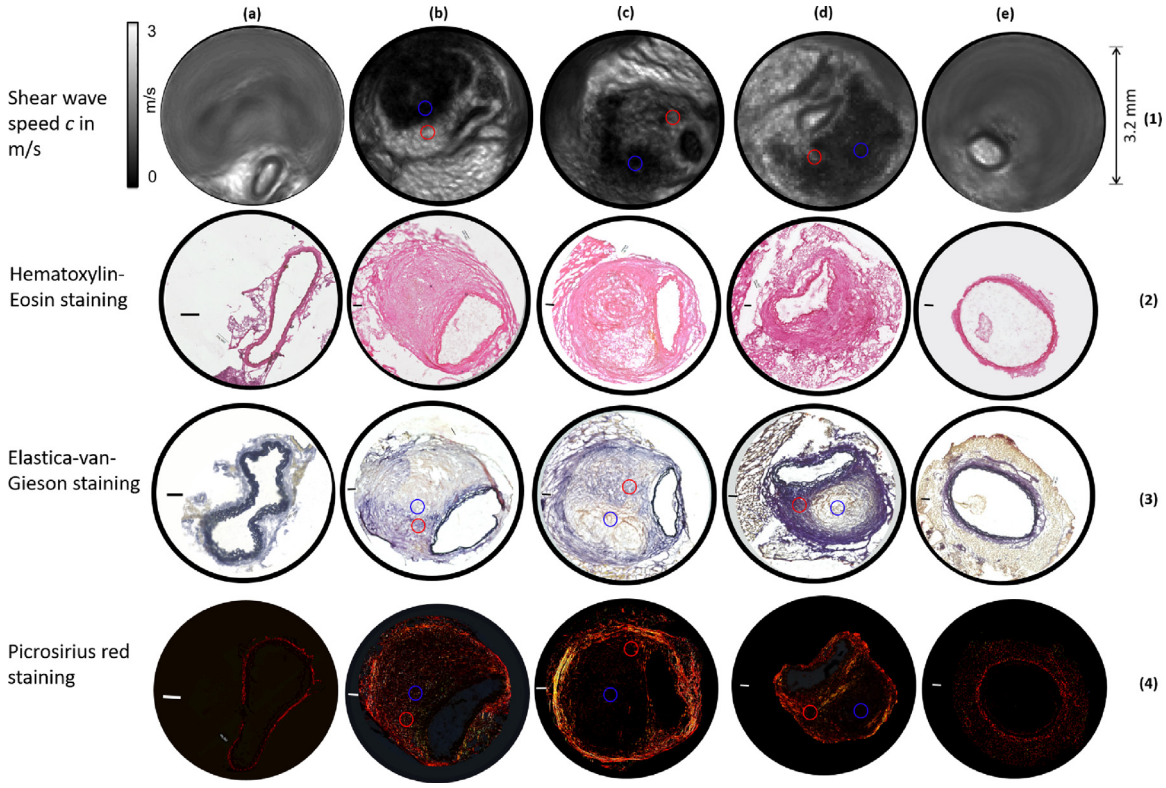

Fig. 4. Extracellular matrix imaging in *ex vivo* µMMRE and histology. Representative shear wave speed (**1**), Hematoxylin-Eosin (**2**), Elastica-van-Gieson (**3**) and Picrosirius red stainings (**4**) of a control aorta (**a**), three different AAA samples with a pronounced thrombus mass (**b–d**) and an AAA that did not develop a thrombus (**e**) are presented. The circles represent extracellular matrix-rich (red) and -poor (blue) ROIs inside the AAA thrombus (**b–d**). The scale bars in the histological images represent 100 µm. *µMMRE* microscopic multifrequency magnetic resonance elastography**,** *AAA* abdominal aortic aneurysm, *ROI* region of interest.

with pronounced inhomogeneity and distinct ECM-rich and ECM-poor regions. The combined information from *ex vivo* μMMRE, EvG and PSR stainings demonstrated a very good correlation of SWS as a stiffness marker with the local distribution and quantity of elastin ($R^2 = 0.79$) and collagen ($R^2 = 0.79$). Consistently, SWS differed significantly ($p < 0.05$) between ECM-rich and ECM-poor regions. These results indicate the importance of high spatial resolution when correlating stiffness with histopathological features towards AAA rupture risk assessment. In addition, it is possible to adapt a similar µMMRE-based approach for analyzing excised human AAAs in the future, similar to other *ex vivo* biomechanical measurement techniques [9].

Literature data on MRE and USE in AAA are sparse, studies have been performed in a porcine model [24] and in patients [27], with a highest spatial in-plane resolution of 3.13 × 6.25 mm. For the longitudinal *ex vivo* animal study [24], AAAs sized in the range between 3 and 12 cm showed 5.8–6.8 kPa stiffness at vibration frequencies of 70 Hz. In the *in vivo* human study [27], the mean stiffness of AAAs was 13.97 ± 4.2 kPa. In agreement with our study, a significant reduction of collagen and elastin due to remodeling of the ECM of AAAs was observed in both studies. For comparison, we can convert the SWS determined in our study to the shear stiffness μ given in [24,27] using the formula: $\mu = SWS^2 \cdot \rho$ (with $\rho = 1000 kg/m^3$ as density of AAA). There are several reasons for the clear difference compared to values of 0.2–1.1 kPa found in our study for AAA stiffness. First, species differ, and physiological parameters vary between *in vivo* and *ex vivo* studies, in particular the blood pressure is an important confounder for vessel wall stiffness [35]. Furthermore, the algorithms used to compute viscoelastic parameters differ. In [24,27] a local-frequency estimation (LFE) inversion algorithm was used while we applied a wave number-based inversion method. Different filter settings for the suppression of pressure waves and noise influence the resulting stiffness values. In addition, the aforementioned studies calculated stiffness values for AAAs as a whole, without differentiating between the thrombus mass and vessel wall. This, and fundamentally methodological differences in data acquisition prevent a comparison with other MRE studies performed on porcine and human aortas addressing stiffness changes due to fixation [29], hypertension [23], cardiac cycle-induced stiffness changes [25], reproducibility [25], and age dependence [27].

Methodological similarities with the present study in the use of multiple vibration frequencies for data acquisition and subsequent calculation of stiffness with the k-MDEV method exist for time-harmonic ultrasound elastography (THE) and multi-frequency MRE (MMRE). For THE, SWS of 2.14 m/s were found for an arterial pressure of 30 mm Hg in a porcine model [36] (vibration frequencies: 60,70, and 80 Hz), and 2.09–2.14 m/s were reported for healthy subjects with an average age of 30 years (vibration frequencies: 60,70, and 80 Hz) [37]. Application of steady state MMRE revealed for abdominal human aortas in healthy subjects with a median age of 33 years SWS of 2.48 m/s (vibration frequencies: 50, 60,70, and 80 Hz) [28]. The lower AAA values in our *ex vivo* mouse model could possibly be related to the observed depletion of ECM components and thus reflect true absolute stiffness values. Nevertheless, we cannot fully exclude the influence of the soft gel matrix in which tissue specimens were embedded on the measured shear wave speed.

Further limitations of our study are: (i) an increase in the number of animals would improve the statistical power of the results. Since only five animals developed an AAA in the experimental group and only three of those developed a pronounced thrombus that could be measured in μMMRE, our results should be viewed as an exploratory work. (ii) The sample preparation protocol could

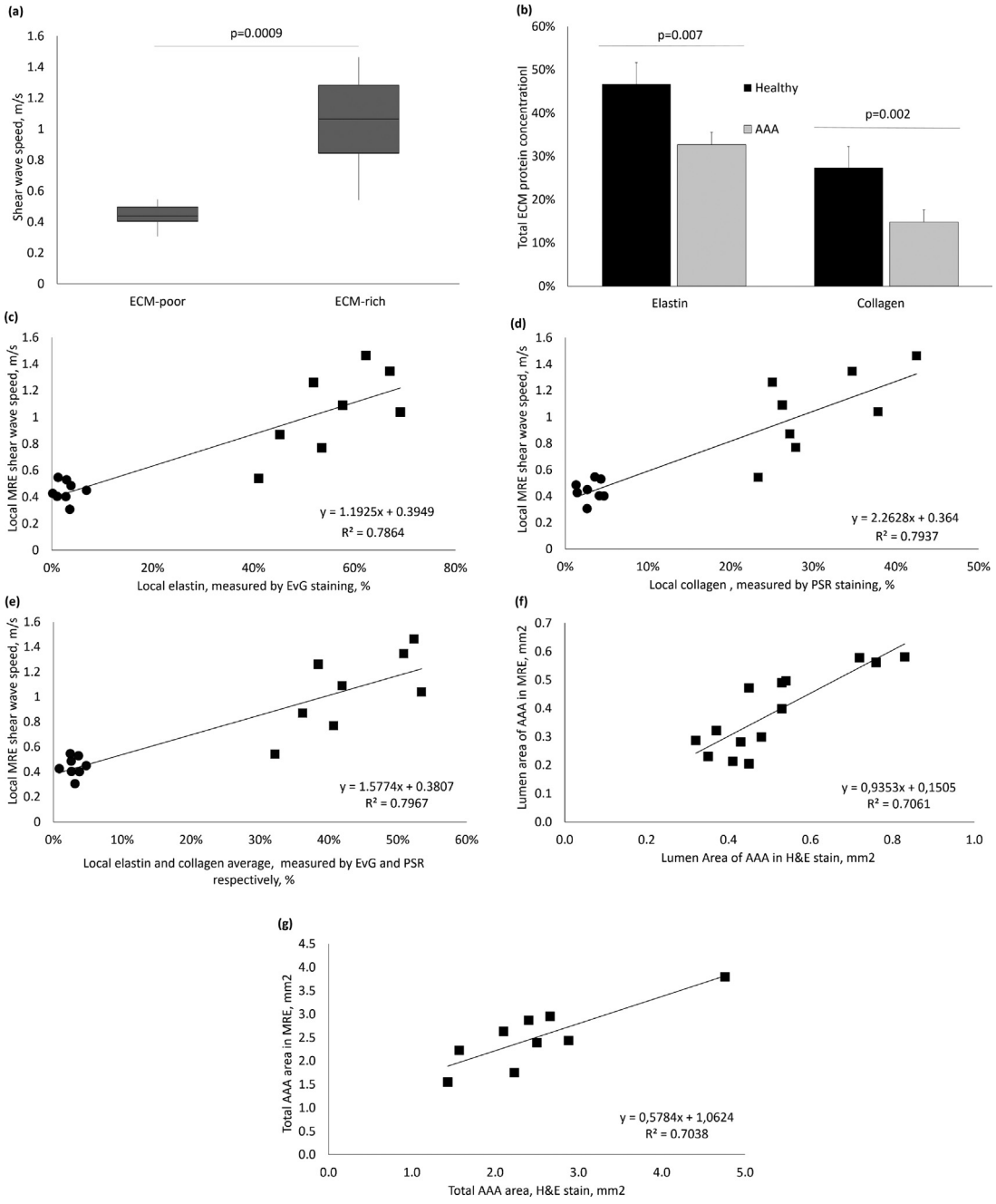

Fig. 5. Correlation of local ROI shear wave speed and extracellular matrix proteins. **(a)** The average shear wave speed in the ECM-poor ROIs of the thrombus was 0.44 m/s while in the ECM-rich ROIs, it reached 1.04 m/s. **(b)** Compared to the control group, the total amount of both elastin and collagen significantly decreased in the AAA group. The local shear wave speed in μMMRE was in great correlation to elastin **(c)** and collagen **(d)** separately and altogether **(e).** The dots in the diagrams in **(c), (d)** and **(e)** indicate ECM-poor ROIs while the squares represent ECM-rich ROIs in the thrombus. (**c-e)** Multiple transversal slides ($n = 8$) from each thrombus-containing AAA were analyzed in order to detect local ECM variations in the thrombus. **(f)** A strong correlation between the aortic lumen area in μMMRE and H&E stain was found ($R^2 = 0.71$). **(g)** The total AAA area including the thrombus also correlated highly ($R^2 = 0.70$). In order to detect local changes in the lumen and total AAA size, we took $n = 14$ **(f)** measurements for lumen size from all samples and $n = 8$ **(g)** for total AAA size from the animals that developed a thrombus, measured as the outer diameter around the adventitia. AAA abdominal aortic aneurysm, μMMRE microscopic multifrequency magnetic resonance elastography, *H&E* hematoxylin-eosin stain, *ROI* region of interest, *ECM* extracellular matrix.

be further optimized, since the aortic lumen partially collapsed in some samples. However, the aneurysmal thrombus was always clearly visible even in the areas with collapsed lumen. (iii) the inclusion of a longitudinal study design would allow to monitor the remodeling of ECM during the AAA development. (iv) the thickness of the murine aortic wall is at the limit of μMMRE imaging resolution, therefore we could only analyze the thrombus and it was not possible to deliver reliable information about the aortic wall during AAA development and progression. (v) the translation of our results on AAAs in the *ex vivo* mouse model to humans is limited. While there is agreement in the fundamental disease mechanisms, e.g. ECM remodeling, hematoma development, and luminal dilatation, differences to the Apo E-/- Ang II mouse model exist in regard to the development of suprarenal dissecting AAAs due to breakage in elastin, whereas humans mostly develop fusiform infrarenal AAAs [61,62]. In our disease model, no calcifications in the thrombus were observed which can lead to a potential overstretching of the noncalcified tissue portions in human

thrombi [54,63]. Furthermore, progression to *in vivo* experiments would be desirable to comply with confounding variables in the body, such as blood pressure and vicinity to other organs and tissues. For this purpose, the examination method must be adapted to the physiological boundary conditions existing in mouse models. These adjustments include synchronizing the μMMRE acquisition technique with heartbeat and respiratory cycle as well as further development of the existing actuator system to be able to induce shear waves with sufficient amplitude in the murine aorta.

5. Conclusion

Using *ex vivo* µMMRE with 40 µm resolution we were able to map stiffness of AAAs in a murine model. Spatially resolved SWS correlated with local ECM remodeling in the aneurysmal thrombus quantified by histological stainings. This study is an important step in assessing tissue stiffness as an image marker sensitive to structural changes during the pathological ECM remodeling in the course of AAAs.

Funding

This work was supported by the Deutsche Forschungsgemeinschaft (DFG, German Research Foundation) Projects CRC 1340 Matrix in Vision; GRK 2260 BIOQIC, MA 5943/3-1/4-1/9-1.

Data availability statement

The datasets generated during and/or analyzed during the current study are available from the corresponding author on reasonable request.

Declaration of Competing Interest

The authors declare that they have no known competing financial interests or personal relationships that could have appeared to influence the work reported in this paper.

CRediT authorship contribution statement

Dilyana B. Mangarova: Conceptualization, Visualization, Formal analysis, Data curation, Writing – original draft, Writing – review & editing. **Gergely Bertalan:** Conceptualization, Visualization, Formal analysis, Data curation. **Jakob Jordan:** Formal analysis, Data curation, Writing – review & editing. **Julia Brangsch:** Conceptualization, Visualization, Formal analysis, Data curation, Writing – review & editing. **Avan Kader:** Writing – review & editing. **Jana Möckel:** Writing – review & editing. **Lisa C. Adams:** Writing – review & editing. **Ingolf Sack:** Writing – review & editing. **Matthias Taupitz:** Writing – review & editing. **Bernd Hamm:** Writing – review & editing. **Marcus R. Makowski:** Conceptualization, Visualization, Writing – original draft, Writing – review & editing. **Jürgen Braun:** Conceptualization, Visualization, Writing – review & editing.

References

[1] W.H. Pearce, C.K. Zarins, J.M. Bacharach, G. American Heart Association Writing, Atherosclerotic peripheral vascular disease symposium II: controversies in abdominal aortic aneurysm repair, Circulation 118 (25) (2008) 2860–2863.
[2] P.S. King, P.L. Cooperberg, S.M. Madigan, The anechoic crescent in abdominal aortic aneurysms: not a sign of dissection, AJR Am. J. Roentgenol. 146 (2) (1986) 345–348.
[3] F. Labruto, L. Blomqvist, J. Swedenborg, Imaging the intraluminal thrombus of abdominal aortic aneurysms: techniques, findings, and clinical implications, J. Vasc. Interv. Radiol. 22 (8) (2011) 1069–1075 quiz 1075.
[4] M. Castrucci, R. Mellone, A. Vanzulli, A. De Gaspari, R. Castellano, D. Astore, R. Chiesa, A. Grossi, A. Del Maschio, Mural thrombi in abdominal aortic aneurysms: MR imaging characterization–useful before endovascular treatment? Radiology 197 (1) (1995) 135–139.
[5] M.R. Law, J. Morris, N.J. Wald, Screening for abdominal aortic aneurysms, J. Med. Screen. 1 (2) (1994) 110–115 discussion 115-6.
[6] D.E. Szilagyi, J.P. Elliott, R.F. Smith, Clinical fate of the patient with asymptomatic abdominal aortic aneurysm and unfit for surgical treatment, Arch. Surg. 104 (4) (1972) 600–606.
[7] W.A. Cappeller, H. Engelmann, S. Blechschmidt, M. Wild, L. Lauterjung, Possible objectification of a critical maximum diameter for elective surgery in abdominal aortic aneurysms based on one- and three-dimensional ratios, J. Cardiovasc. Surg. 38 (6) (1997) 623–628 (Torino).
[8] F.A. Lederle, G.R. Johnson, S.E. Wilson, D.J. Ballard, W.D. Jordan Jr., J. Blebea, F.N. Littooy, J.A. Freischlag, D. Bandyk, J.H. Rapp, A.A. Salam, I. Veterans Affairs Cooperative Study, Rupture rate of large abdominal aortic aneurysms in patients refusing or unfit for elective repair, JAMA 287 (22) (2002) 2968–2972.
[9] D.A. Vorp, J.P. Vande Geest, Biomechanical determinants of abdominal aortic aneurysm rupture, Arterioscler. Thromb. Vasc. Biol. 25 (8) (2005) 1558–1566.
[10] R.P. Mecham, Overview of extracellular matrix, Curr. Protoc. Cell Biol. 00 (1) (1998).
[11] J.E. Wagenseil, R.P. Mecham, Vascular extracellular matrix and arterial mechanics, Physiol. Rev. 89 (3) (2009) 957–989.
[12] F.A. Hellenthal, W.A. Buurman, W.K. Wodzig, G.W. Schurink, Biomarkers of AAA progression. Part 1: extracellular matrix degeneration, Nat. Rev. Cardiol. 6 (7) (2009) 464–474.
[13] N. Sakalihasan, A. Heyeres, B.V. Nusgens, R. Limet, C.M. Lapiére, Modifications of the extracellular matrix of aneurysmal abdominal aortas as a function of their size, Eur. J. Vasc. Surg. 7 (6) (1993) 633–637.
[14] J. Leach, E. Kao, C. Zhu, D. Saloner, M.D. Hope, On the relative impact of intraluminal thrombus heterogeneity on abdominal aortic aneurysm mechanics, J. Biomech. Eng. (2019).
[15] E. Di Martino, S. Mantero, F. Inzoli, G. Melissano, D. Astore, R. Chiesa, R. Fumero, Biomechanics of abdominal aortic aneurysm in the presence of endoluminal thrombus: Experimental characterisation and structural static computational analysis, Eur. J. Vasc. Endovasc. 15 (4) (1998) 290–299.
[16] W.R. Mower, W.J. Quiñones, S.S. Gambhir, Effect of intraluminal thrombus on abdominal aortic aneurysm wall stress, J. Vasc. Surg. 26 (4) (1997) 602–608.
[17] J.B. Michel, J.L. Martin-Ventura, J. Egido, N. Sakalihasan, V. Treska, J. Lindholt, E. Allaire, U. Thorsteinsdottir, G. Cockerill, J. Swedenborg, F.E. consortium, Novel aspects of the pathogenesis of aneurysms of the abdominal aorta in humans, Cardiovasc. Res. 90 (1) (2011) 18–27.
[18] D.A. Vorp, P.C. Lee, D.H. Wang, M.S. Makaroun, E.M. Nemoto, S. Ogawa, M.W. Webster, Association of intraluminal thrombus in abdominal aortic aneurysm with local hypoxia and wall weakening, J. Vasc. Surg. 34 (2) (2001) 291–299.
[19] S. Polzer, T.C. Gasser, J. Swedenborg, J. Bursa, The impact of intraluminal thrombus failure on the mechanical stress in the wall of abdominal aortic aneurysms, Eur. J. Vasc. Endovasc. Surg. 41 (4) (2011) 467–473.
[20] S. Hirsch, J. Braun, I. Sack, Magnetic Resonance Elastography: Physical Background and Medical Applications, Wiley-VCH Verlag GmbH & Co. KGaA, 2017.
[21] J. Mura, F. Schrank, I. Sack, An analytical solution to the dispersion-by-inversion problem in magnetic resonance elastography, Magn. Reson. Med. 84 (1) (2020) 61–71.
[22] H. Dong, N. Jin, S. Kannengiesser, B. Raterman, R.D. White, A. Kolipaka, Magnetic resonance elastography for estimating *in vivo* stiffness of the abdominal aorta using cardiac-gated spin-echo echo-planar imaging: a feasibility study, NMR Biomed. 34 (1) (2021) e4420.
[23] H. Dong, R. Mazumder, V.S.P. Illapani, X. Mo, R.D. White, A. Kolipaka, *In vivo* quantification of aortic stiffness using MR elastography in hypertensive porcine model, Magn. Reson. Med. 78 (6) (2017) 2315–2321.
[24] H. Dong, D.S. Russell, A.S. Litsky, M.E. Joseph, X. Mo, R.D. White, A. Kolipaka, *In vivo* aortic magnetic resonance elastography in abdominal aortic aneurysm: a validation in an animal model, Invest. Radiol. 55 (7) (2020) 463–472.
[25] W.E. Kenyhercz, B. Raterman, V.S. Illapani, J. Dowell, X. Mo, R.D. White, A. Kolipaka, Quantification of aortic stiffness using magnetic resonance elastography: Measurement reproducibility, pulse wave velocity comparison, changes over cardiac cycle, and relationship with age, Magn. Reson. Med. 75 (5) (2016) 1920–1926.
[26] A. Kolipaka, V.S. Illapani, P. Kalra, J. Garcia, X. Mo, M. Markl, R.D. White, Quantification and comparison of 4D-flow MRI-derived wall shear stress and MRE-derived wall stiffness of the abdominal aorta, J. Magn. Reson. Imaging 45 (3) (2017) 771–778.
[27] A. Kolipaka, V.S. Illapani, W. Kenyhercz, J.D. Dowell, M.R. Go, J.E. Starr, P.S. Vaccaro, R.D. White, Quantification of abdominal aortic aneurysm stiffness using magnetic resonance elastography and its comparison to aneurysm diameter, J. Vasc. Surg. 64 (4) (2016) 966–974.
[28] L.A. Schaafs, F. Schrank, C. Warmuth, I.G. Steffen, J. Braun, B. Hamm, I. Sack, T. Elgeti, Steady-state multifrequency magnetic resonance elastography of the thoracic and abdominal human aorta-validation and reference values, Invest. Radiol. 55 (7) (2020) 451–456.
[29] N. Zhang, J. Chen, M. Yin, K.J. Glaser, L. Xu, R.L. Ehman, Quantification of regional aortic stiffness using MR elastography: a phantom and *ex-vivo* porcine aorta study, Magn. Reson. Imaging 34 (2) (2016) 91–96.
[30] A.R. Damughatla, B. Raterman, T. Sharkey-Toppen, N. Jin, O.P. Simonetti, R.D. White, A. Kolipaka, Quantification of aortic stiffness using MR elastog-

raphy and its comparison to MRI-based pulse wave velocity, J. Magn. Reson. Imaging 41 (1) (2015) 44–51.
[31] A. Kolipaka, D. Woodrum, P.A. Araoz, R.L. Ehman, MR elastography of the *in vivo* abdominal aorta: a feasibility study for comparing aortic stiffness between hypertensives and normotensives, J. Magn. Reson. Imaging 35 (3) (2012) 582–586.
[32] L. Marais, M. Pernot, H. Khettab, M. Tanter, E. Messas, M. Zidi, S. Laurent, P. Boutouyrie, Arterial stiffness assessment by shear wave elastography and ultrafast pulse wave imaging: comparison with reference techniques in normotensives and hypertensives, Ultrasound Med. Biol. 45 (3) (2019) 758–772.
[33] E.J.S. Mascarenhas, M.F.J. Peters, J. Nijs, M.C.M. Rutten, F.N. van de Vosse, R.G.P. Lopata, Assessment of mechanical properties of porcine aortas under physiological loading conditions using vascular elastography, J. Mech. Behav. Biomed. Mater. 59 (2016) 185–196.
[34] L.A. Schaafs, H. Tzschatzsch, C. Figiel, M. van der Giet, A. Reshetnik, B. Hamm, I. Sack, T. Elgeti, Quantitative time-harmonic ultrasound elastography of the abdominal aorta and inferior vena cava, Ultrasound Med. Biol. 45 (9) (2019) 2349–2355.
[35] L.A. Schaafs, H. Tzschatzsch, A. Reshetnik, M. van der Giet, J. Braun, B. Hamm, I. Sack, T. Elgeti, Ultrasound time-harmonic elastography of the aorta: effect of age and hypertension on aortic stiffness, Invest. Radiol. 54 (11) (2019) 675–680.
[36] L.A. Schaafs, H. Tzschatzsch, I.G. Steffen, J. Braun, B. Hamm, I. Sack, T. Elgeti, Quantification of aortic stiffness by ultrasound time-harmonic elastography: the effect of intravascular pressure on elasticity measures in a porcine model, Invest. Radiol. 55 (3) (2020) 174–180.
[37] L.A. Schaafs, H. Tzschatzsch, M. van der Giet, A. Reshetnik, I.G. Steffen, B. Hamm, J. Braun, I. Sack, T. Elgeti, Time-harmonic ultrasound elastography of the descending abdominal aorta: initial results, Ultrasound Med. Biol. 43 (11) (2017) 2550–2557.
[38] C. Schmitt, A. Hadj Henni, G. Cloutier, Ultrasound dynamic micro-elastography applied to the viscoelastic characterization of soft tissues and arterial walls, Ultrasound Med. Biol. 36 (9) (2010) 1492–1503.
[39] E.M.J. van Disseldorp, N.J. Petterson, F.N. van de Vosse, M. van Sambeek, R.G.P. Lopata, Quantification of aortic stiffness and wall stress in healthy volunteers and abdominal aortic aneurysm patients using time-resolved 3D ultrasound: a comparison study, Eur. Heart J. Cardiovasc. Imaging 20 (2) (2019) 185–191.
[40] E. Widman, E. Maksuti, C. Amador, M.W. Urban, K. Caidahl, M. Larsson, Shear wave elastography quantifies stiffness in *ex vivo* porcine artery with stiffened arterial region, Ultrasound Med. Biol. 42 (10) (2016) 2423–2435.
[41] Y. Jamin, J.K.R. Boult, J. Li, S. Popov, P. Garteiser, J.L. Ulloa, C. Cummings, G. Box, S.A. Eccles, C. Jones, J.C. Waterton, J.C. Bamber, R. Sinkus, S.P. Robinson, Exploring the biomechanical properties of brain malignancies and their pathologic determinants *in vivo* with magnetic resonance elastography, Cancer Res. 75 (7) (2015) 1216–1224.
[42] K. Schregel, E. Wuerfel, P. Garteiser, I. Gemeinhardt, T. Prozorovski, O. Aktas, H. Merz, D. Petersen, J. Wuerfel, R. Sinkus, Demyelination reduces brain parenchymal stiffness quantified *in vivo* by magnetic resonance elastography, Proc. Natl. Acad. Sci. U.S.A. 109 (17) (2012) 6650–6655.
[43] S.F. Othman, H. Xu, T.J. Royston, R.L. Magin, Microscopic magnetic resonance elastography (microMRE), Magn. Reson. Med. 54 (3) (2005) 605–615.
[44] G. Bertalan, J. Guo, H. Tzschatzsch, C. Klein, E. Barnhill, I. Sack, J. Braun, Fast tomoelastography of the mouse brain by multifrequency single-shot MR elastography, Magn. Reson. Med. 81 (4) (2019) 2676–2687.
[45] H. Tzschatzsch, J. Guo, F. Dittmann, S. Hirsch, E. Barnhill, K. Johrens, J. Braun, I. Sack, Tomoelastography by multifrequency wave number recovery from time-harmonic propagating shear waves, Med. Image Anal. 30 (2016) 1–10.
[46] J. Brangsch, C. Reimann, J.O. Kaufmann, L.C. Adams, D.C. Onthank, C. Thone-Reineke, S.P. Robinson, R. Buchholz, U. Karst, R.M. Botnar, B. Hamm, M.R. Makowski, Concurrent molecular magnetic resonance imaging of inflammatory activity and extracellular matrix degradation for the prediction of aneurysm rupture, Circ. Cardiovasc. Imaging 12 (3) (2019) e008707.
[47] L.C. Adams, J. Brangsch, C. Reimann, J.O. Kaufmann, R. Buchholz, U. Karst, R.M. Botnar, B. Hamm, M.R. Makowski, Simultaneous molecular MRI of extracellular matrix collagen and inflammatory activity to predict abdominal aortic aneurysm rupture, Sci. Rep. 10 (1) (2020) 15206.
[48] H. Lu, D.A. Howatt, A. Balakrishnan, J.J. Moorleghen, D.L. Rateri, L.A. Cassis, A. Daugherty, Subcutaneous angiotensin ii infusion using osmotic pumps induces aortic aneurysms in mice, J. Vis. Exp. (103) (2015).
[49] N. Robbins, A. Thompson, A. Mann, A.L. Blomkalns, Isolation and excision of murine aorta; a versatile technique in the study of cardiovascular disease, J. Vis. Exp. (93) (2014) e52172.
[50] Y. Nakashima, A.S. Plump, E.W. Raines, J.L. Breslow, R. Ross, ApoE-deficient mice develop lesions of all phases of atherosclerosis throughout the arterial tree, Arterioscler. Thromb. 14 (1) (1994) 133–140.
[51] J. Jordan, G. Bertalan, T. Meyer, H. Tzschätzsch, A. Gauert, L. Bramè, H. Herthum, Y. Safraou, L. Schröder, J. Braun, A.H. Hagemann, I. Sack, Microscopic multifrequency MR elastography for mapping viscoelasticity in zebrafish, Magn. Reson. Med. (2021).
[52] S. Jana, M. Hu, M. Shen, Z. Kassiri, Extracellular matrix, regional heterogeneity of the aorta, and aortic aneurysm, Exp. Mol. Med. 51 (12) (2019) 1–15.
[53] J.E. Wagenseil, R.P. Mecham, Elastin in large artery stiffness and hypertension, J. Cardiovasc. Transl. Res. 5 (3) (2012) 264–273.
[54] H.E. Barrett, E.M. Cunnane, H. Hidayat, J.M. O'Brien, M.A. Moloney, E.G. Kavanagh, M.T. Walsh, On the influence of wall calcification and intraluminal thrombus on prediction of abdominal aortic aneurysm rupture, J. Vasc. Surg. 67 (4) (2018) 1234-1246 e2.
[55] J. Tong, T. Cohnert, P. Regitnig, G.A. Holzapfel, Effects of age on the elastic properties of the intraluminal thrombus and the thrombus-covered wall in abdominal aortic aneurysms: biaxial extension behavior and material modeling, Eur. J. Vasc. Endovasc. Surg. 42 (2) (2011) 207–219.
[56] R. Adolph, D.A. Vorp, D.L. Steed, M.W. Webster, M.V. Kameneva, S.C. Watkins, Cellular content and permeability of intraluminal thrombus in abdominal aortic aneurysm, J. Vasc. Surg. 25 (5) (1997) 916–926.
[57] I. Wiernicki, M. Cnotliwy, I. Baranowska-Bosiacka, E. Urasinska, A. Kwas, J. Bober, P. Gutowski, Elastin degradation within the abdominal aortic aneurysm wall - relationship between intramural pH and adjacent thrombus formation, Eur. J. Clin. Invest. 38 (12) (2008) 883–887.
[58] A. Lukasiewicz, J. Reszec, R. Kowalewski, L. Chyczewski, U. Lebkowska, Assessment of inflammatory infiltration and angiogenesis in the thrombus and the wall of abdominal aortic aneurysms on the basis of histological parameters and computed tomography angiography study, Folia. Histochem. Cytobiol. 50 (4) (2012) 547–553.
[59] S.J. Haller, J.D. Crawford, K.M. Courchaine, C.J. Bohannan, G.J. Landry, G.L. Moneta, A.F. Azarbal, S. Rugonyi, Intraluminal thrombus is associated with early rupture of abdominal aortic aneurysm, J. Vasc. Surg. 67 (4) (2018) 1051-1058 e1.
[60] M. Kazi, J. Thyberg, P. Religa, J. Roy, P. Eriksson, U. Hedin, J. Swedenborg, Influence of intraluminal thrombus on structural and cellular composition of abdominal aortic aneurysm wall, J. Vasc. Surg. 38 (6) (2003) 1283–1292.
[61] A. Daugherty, M.W. Manning, L.A. Cassis, Angiotensin II promotes atherosclerotic lesions and aneurysms in apolipoprotein E-deficient mice, J. Clin. Invest. 105 (11) (2000) 1605–1612.
[62] K. Saraff, F. Babamusta, L.A. Cassis, A. Daugherty, Aortic dissection precedes formation of aneurysms and atherosclerosis in angiotensin II-infused, apolipoprotein E-deficient mice, Arterioscler. Thromb. Vasc. Biol. 23 (9) (2003) 1621–1626.
[63] Z.Y. Li, J. U-King-Im, T.Y. Tang, E. Soh, T.C. See, J.H. Gillard, Impact of calcification and intraluminal thrombus on the computed wall stresses of abdominal aortic aneurysm, J. Vasc. Surg. 47 (5) (2008) 928–935.